Evolution of quantum superoscillations and optical superresolution without evanescent waves

INSTITUTE OF PHYSICS PUBLISHING JOURNAL OF PHYSICS A: MATHEMATICAL AND GENERAL

J. Phys. A: Math. Gen. **39** (2006) 6965–6977 doi:10.1088/0305-4470/39/22/011

Evolution of quantum superoscillations and optical superresolution without evanescent waves

M V Berry[1,3] **and S Popescu**[1,2]

[1] H H Wills Physics Laboratory, Tyndall Avenue, Bristol BS8 1TL, UK
[2] Hewlett-Packard Laboratories, Stoke Gifford, Bristol, BS12 6QZ, UK

Received 15 February 2006, in final form 11 April 2006
Published 16 May 2006
Online at stacks.iop.org/JPhysA/39/6965

Abstract

A superoscillatory function—that is, a band-limited function $f(x)$ oscillating faster than its fastest Fourier component—is taken to be the initial state of a freely-evolving quantum wavefunction ψ. The superoscillations persist for unexpectedly long times, but eventually disappear through the interaction of contributions to ψ with complex momenta that are exponentially disparate in magnitude; this is established by applying the asymptotics of integrals, supported by numerics. $f(x)$ can alternatively be regarded as the wave generated by a diffraction grating, propagating paraxially and without evanescence as ψ in the space beyond. The persistence of superoscillations is then interpreted as the propagation of sub-wavelength structure farther into the field than the more familiar evanescent waves.

PACS numbers: 02.30.Mv, 06.35.Ge, 42.25.Fx, 42.30.Kq

1. Introduction

Physical and mathematical arguments [1–10] have established the existence of band-limited functions $f(x)$ with the apparently paradoxical property that they can oscillate faster than their fastest Fourier component; moreover, these 'superoscillations' can be arbitrarily fast and can occupy arbitrarily large regions of the x axis. The paradox posed by superoscillations is dissolved [6] by $f(x)$ being exponentially small in the superoscillatory region.

Our purpose here is to explore the following question: how long do superoscillations survive if $f(x)$ is the initial state of a quantum wavefunction $\psi(x,t)$ evolving in free space? The naive expectation, that superoscillations are so delicate that they will dissolve in an exponentially short time, turns out to be wrong: the fast variations of ψ persist much longer.

For our detailed study we choose not a general superoscillatory $f(x)$—constructed, for example, by the recipes in [6] or [9, 10]. Rather, we consider one particular function, described in section 2; but we expect this to display general features. The evolution of the state, starting

[3] http://www.phy.bris.ac.uk/people/berry_mv/index.html.

with $f(x)$, is formulated and illustrated numerically in section 3. The detailed explanation (section 4) of the persistence of the superoscillations involves the interaction of waves with complex momenta, derived by a delicate exercise in the asymptotics of integrals.

Since the time-dependent Schrödinger equation for the evolution of a function of one variable x is identical to the paraxial wave equation in the plane, and because the $f(x)$ we study is periodic, our evolving quantum state also describes waves (e.g. light) propagating beyond a suitably constructed diffraction grating. As explained in section 5, this grating can generate a wave with a structure smaller than the wavelength, and so represents a kind of 'superresolution'. We show that this superresolution persists over much greater distances than the usual kind based on evanescent waves; moreover, this potentially useful property survives the replacement of paraxial by exact wave propagation.

2. Superoscillatory initial state

Consider the function [1, 7]

$$f(x) = (\cos x + \mathrm{i}a \sin x)^N \qquad (a > 1, N \gg 1). \tag{1}$$

For general a, $f(x)$ is periodic with period π (up to a sign if N is odd). If $a = 1$, $f(x) = \exp(\mathrm{i}Nx)$, representing a plane wave travelling to the right. For $a > 1$, the variation near $x = 0$ is faster:

$$f(x) \approx \exp(N \log(1 + \mathrm{i}ax) \approx \exp(\mathrm{i}aNx). \tag{2}$$

This is surprising because the Fourier series for $f(x)$, namely

$$f(x) = \sum_{m=0}^{N} c_m \exp\{\mathrm{i}Nk_m x\}, \tag{3}$$

where

$$k_m = 1 - \frac{2m}{N}, \qquad c_m = \frac{N!}{2^N}(-1)^m \frac{(a^2-1)^{N/2}[(a-1)/(a+1)]^{Nk_m/2}}{[N(1+k_m)/2]![N(1-k_m)/2]!}, \tag{4}$$

contains only wavenumbers $|k_m| \leqslant 1$. Therefore equation (2) indicates superoscillatory behaviour, with the degree of superoscillation described by a.

To understand the superoscillations in greater detail, we write $f(x)$ in a form that can be confirmed by direct calculation, namely

$$f(x) = \left(\frac{a}{k(x)}\right)^{N/2} \exp\left\{\mathrm{i}N \int_0^x \mathrm{d}x'\, k(x')\right\}, \tag{5}$$

involving the local wavenumber (expectation of momentum)

$$k(x) \equiv \frac{1}{N} \operatorname{Im} \partial_x \log f(x) = \frac{a}{\cos^2 x + a^2 \sin^2 x}. \tag{6}$$

The wavenumber varies from the superoscillatory $k(0) = a$ to the slowest variation $k(\pi) = 1/a$. The superoscillatory region, within which $|k| > 1$, is

$$|x| < x_s = \operatorname{arccot}\sqrt{a}. \tag{7}$$

The number of oscillations in this region is

$$n_{\mathrm{osc}} = \frac{N}{2\pi} \int_{-\operatorname{arccot}\sqrt{a}}^{\operatorname{arccot}\sqrt{a}} \mathrm{d}x\, k(x) = \frac{N}{2\pi} \arctan\sqrt{a}. \tag{8}$$

Equation (5) shows that in the superoscillatory region $|f|$ is exponentially smaller (in N) than in the 'normal' region $|k| < 1$. Therefore, N is an asymptotic parameter, describing the number

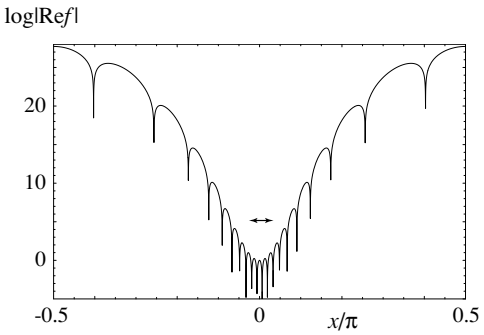

Figure 1. The superoscillatory function $f(x)$ (equation (1)), plotted as $\log|\mathrm{Re}\, f|$ for $a = 4$, $N = 20$. Here and in subsequent figures, double-headed arrows mark the shortest period $\pi/N = \pi/20$ in the Fourier series; because $a = 4$, the fastest superoscillations (near $x = 0$) are four times smaller.

of oscillations in the superoscillatory region and the corresponding exponential smallness of $|f|$.

The region where (2) is a good approximation, that is, where the amplitude of the superoscillations is approximately constant—we can call this the region of fast superoscillations—is smaller than (7). To explore it, we expand (5) near $x = 0$, using (6), to get an approximation slightly more accurate than (2):

$$f(x) \approx \exp\{\mathrm{i}aNx\} \exp\left\{\tfrac{1}{2}N(a^2-1)x^2\right\}. \tag{9}$$

Thus, the region of fast superoscillations is

$$|x| < x_{\mathrm{fs}} = \frac{1}{\sqrt{N(a^2-1)}}, \tag{10}$$

and the number of fast superoscillations is

$$n_{\mathrm{fs}} = \frac{\sqrt{N}}{\pi}\frac{a}{\sqrt{a^2-1}}. \tag{11}$$

Figure 1 is a picture of $f(x)$, using a representation that will be employed extensively in what follows. To display the oscillations, and to accommodate the exponentially large variation in $|f|$ we plot $\log|\mathrm{Re}\, f|$, so that the oscillations are visible as downward spikes at the zeros of $\mathrm{Re}\, f$ (pictures are very similar with $\mathrm{Im}\, f$ rather than $\mathrm{Re}\, f$).

Superoscillation is a subtle phenomenon, associated with delicate correlations between the Fourier components of $f(x)$. Therefore, there is no hint of superoscillations in the power spectrum, namely

$$P(k) = \frac{Nc_m^2\ (m = (1-k)N/2)}{2\sum_0^N c_m^2} \underset{N\gg 1}{\approx} \frac{1}{\sigma\sqrt{2\pi}} \exp\left\{-\frac{(k-\langle k\rangle)^2}{2\sigma^2}\right\}, \tag{12}$$

where

$$\langle k\rangle = \frac{1}{a}, \qquad \sigma \equiv \sqrt{(k-\langle k\rangle)^2} = \sqrt{\frac{a^2-1}{2Na^2}}. \tag{13}$$

Thus the asymptotic spectrum is a narrow Gaussian (figure 2) centred on the wavenumber $k = 1/a$, representing the exponentially dominant slow oscillations near $|x| = \pi$.

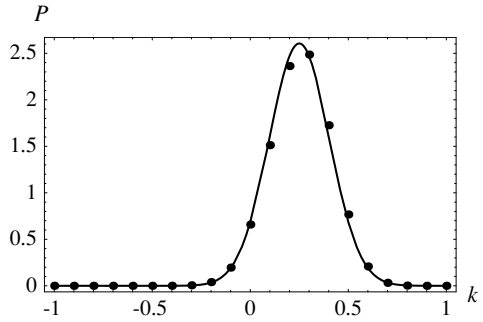

Figure 2. Spectrum of $f(x)$ for $a = 4$, $N = 20$. Dots: the exact spectrum (middle member of (12)); smooth curve: Gaussian approximation (right-hand member of (12)).

3. Quantum evolution and disappearance of superoscillations

It is convenient to write the Schrödinger equation, with initial state $f(x)$, in the form

$$\mathrm{i}N\partial_t\psi(x,t) = -\tfrac{1}{2}\partial_x^2\psi(x,t), \qquad \psi(x,0) = f(x), \tag{14}$$

in which the asymptotic parameter N plays a role analogous to Planck's constant. The evolving state $\psi(x,t)$ can be written either as an integral over the propagator or a sum over Fourier components:

$$\begin{aligned}\psi(x,t) &= \sqrt{\frac{N}{2\pi\mathrm{i}t}}\int_{-\infty}^{\infty}\mathrm{d}x' f(x')\exp\{\mathrm{i}N(x-x')^2/2t\} \\ &= \sum_{m=0}^{N} c_m \exp\left\{\mathrm{i}N\left(k_m x - \frac{1}{2}k_m^2 t\right)\right\}.\end{aligned} \tag{15}$$

Although we will be mainly concerned with the early development of ψ, an important additional property is that ψ is periodic in t as well as in x, with period $N\pi/2$ (up to a phase factor, and a shift in x of $\pi/2$ if N is even). This periodicity is the phenomenon of quantum revivals [11–13].

The white lines in figure 3 show how the oscillations evolve. As figure 3(*a*) shows, the superoscillations do not disappear immediately, but persist for a time. After longer times (figure 3(*b*)) the oscillations get slower, and eventually (figure 3(*c*)) are within the range $|k| \leqslant 1$ expected on the basis of the Fourier components in equations (3) and (4), with the initial region of exponentially weak superoscillations disappearing into a confusion of white at the bottom of the picture. Over the full range between $t = 0$ and the revival period $t = N\pi/2$ (figure 3(*d*)), the oscillations are slower still, reflecting the mean $\langle k\rangle = 1/a$ in the narrow power spectrum (12).

Figure 4 illustrates the disappearance of superoscillations in more detail, with graphs of $\psi(x,t)$ for series of values of t; the value $(3+\sqrt{7})/8$ in figure 4(*d*) is the time when, according to the theory of section 4 applied to this case, the superoscillations have disappeared. A striking feature of figures 4(*c*)–(*e*) is a 'wall', separating regions of fast oscillation (to the left) from much slower oscillations (to the right).

4. Explanation in terms of complex momenta

To understand the disappearance of superoscillations and the 'wall' phenomenon just described, we need a representation of ψ more transparent than the Fourier series (15).

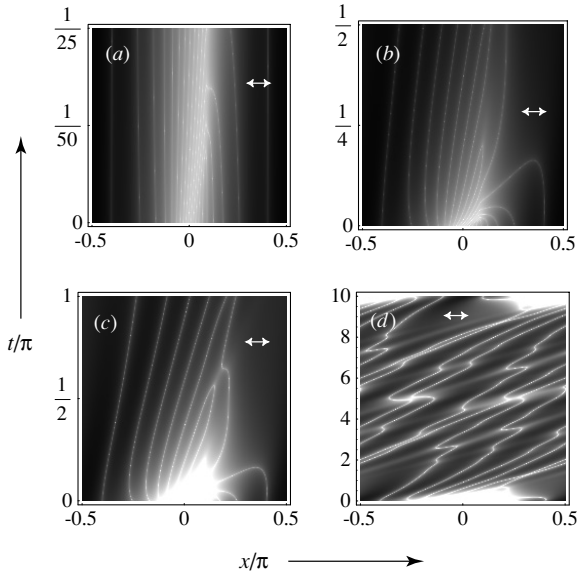

Figure 3. Density plots of $-\log|\mathrm{Re}\ \psi|$ of the evolution of the wavefunction (15), for $a = 4$, $N = 20$. (*a*) $0 \leqslant t \leqslant 0.04\pi$; (*b*) $0 \leqslant t \leqslant \pi/2$, (*c*) $0 \leqslant t \leqslant \pi$; (*d*) $0 \leqslant t \leqslant 10\pi$. In this representation, the zeros of Re ψ appear as white lines.

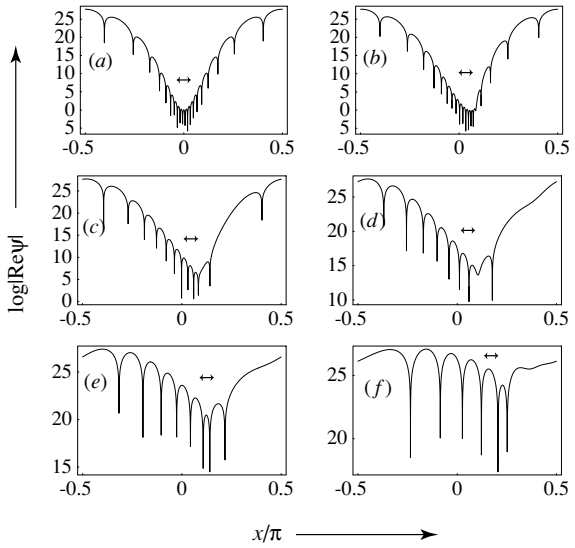

Figure 4. Superoscillations disappearing as t increases, for $a = 4$, $N = 20$. (*a*) $t = 0$; (*b*) $t = 0.015\pi$; (*c*) $t = 0.08\pi$; (*d*) $t = (3 + \sqrt{7})/8 = 0.706$; (*e*) $t = 0.5\pi$; (*f*) $t = \pi$.

This can be derived using asymptotics exploiting $N \gg 1$, which implies that the integrand in (15) varies rapidly in both modulus and phase. To accommodate this, it is convenient to rewrite (15) first as

$$\psi(x,t) = \sqrt{\frac{N}{2\pi i t}} \int_{-\infty}^{\infty} \mathrm{d}x' \exp\left\{ iN \left[\int_0^{x'} \mathrm{d}x'' q(x'') + (x - x')^2/2t \right] \right\}, \quad (16)$$

in which, $q(x)$ is the complex momentum

$$q(x) = -\frac{\mathrm{i}}{N}\partial_x \log f(x) = \frac{a\cos x + \mathrm{i}\sin x}{\cos x + \mathrm{i}a\sin x} \tag{17}$$

(the wavenumber (6) is thus $k(x) = \mathrm{Re}\, q(x)$). And denoting the exponent (complex phase) by $N\Phi$, ψ can be written as

$$\psi(x,t) = \sqrt{\frac{N}{2\pi \mathrm{i}t}} \int_{-\infty}^{\infty} \mathrm{d}x' \exp\{\mathrm{i}N\Phi(x',x,t)\}. \tag{18}$$

For $N \gg 1$, the integral can be approximated by the saddle-point method [14, 15], giving ψ as one or more contributions from the (generally complex) saddles $x_j(x,t)$ (stationary points of Φ), satisfying

$$\partial_{x'}\Phi(x',x,t) = 0 \quad \Rightarrow \quad q(x') = \frac{x-x'}{t} \quad \Rightarrow \quad x' = x_j(x,t). \tag{19}$$

Physically, the saddles can be regarded as complex momenta determining ψ as a superposition of waves, given by standard saddle-point theory as

$$\psi_{\mathrm{sp}}(x,t) = \sum_j \frac{f(x_j)}{\sqrt{1+t\partial_x q(x_j)}} \exp\{\mathrm{i}N(x-x_j)^2/2t\}. \tag{20}$$

The sum is over all the saddles that contribute—that is, all those into which the initial x' contour (the real axis) can be deformed while keeping the integral convergent. For very small t, there is just one contributing saddle, which from (19) is close to x; as t increases, other saddles enter the picture, in a complicated way that we will describe soon and which is essential to understanding how superoscillations disappear.

The saddle-point method can be implemented numerically, giving results almost indistinguishable from those (e.g. figures 3 and 4) computed from the Fourier series, even when N is quite small. But to implement the procedure analytically we introduce a further simplification, exploiting the fact that the phenomenon we are interested in—the disappearance of superoscillations—involves quite small x and t. In this situation, which turns out to be a good approximation for large a, we can replace $f(x)$ and $q(x)$ by simpler functions, and introduce new scaled variables:

$$f_{\mathrm{app}}(\xi) = (1+\mathrm{i}\xi)^N, \qquad q_{\mathrm{app}}(\xi) = \frac{1}{1+\mathrm{i}\xi}, \qquad \xi \equiv ax, \qquad \tau \equiv a^2 t. \tag{21}$$

The scaling eliminates the parameter a from $\psi(\xi,\tau)$ which is given by

$$\begin{aligned}
\psi_{\mathrm{app}}(\xi,\tau) &= \sqrt{\frac{N}{2\pi\mathrm{i}\tau}} \int_{-\infty}^{\infty} \mathrm{d}\xi' f_{\mathrm{app}}(\xi') \exp\{\mathrm{i}N(\xi-\xi')^2/2\tau\} \\
&= \sqrt{\frac{N}{2\pi\mathrm{i}\tau}} \int_{-\infty}^{\infty} \mathrm{d}\xi' \exp\left\{\mathrm{i}N\left[\int_0^{\xi'} \mathrm{d}\xi'' q_{\mathrm{app}}(\xi'') + (\xi-\xi')^2/2\tau\right]\right\} \\
&= \sqrt{\frac{N}{2\pi\mathrm{i}\tau}} \int_{-\infty}^{\infty} \mathrm{d}\xi' \exp\{\mathrm{i}N\Phi_{\mathrm{app}}(\xi',\xi,\tau)\} \\
&= N!(1+\mathrm{i}\xi)^N \sum_{m=0}^{\mathrm{int}(N/2)} \frac{1}{m!(N-2m)!}\left(-\frac{2\mathrm{i}\tau}{N(1+\mathrm{i}\xi)^2}\right)^m.
\end{aligned} \tag{22}$$

Before proceeding further, it is necessary to check that the simplification (21) preserves the essential structure of the wave $\psi(x,t)$ that we are studying. Figure 5 indicates that it does, and that the agreement persists for times over which the superoscillations disappear (there are slight differences, but nothing important).

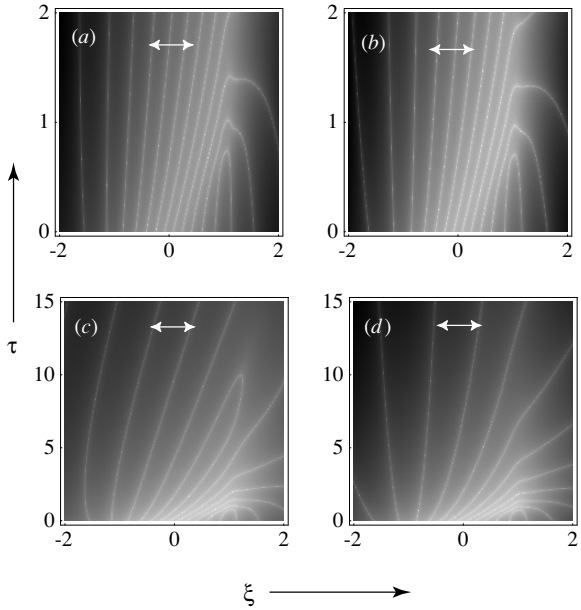

Figure 5. Magnified density plots comparing $-\log|\mathrm{Re}\ \psi|$, computed from (15) ((*a*) and (*c*)) and $-\log|\mathrm{Re}\ \psi_{\mathrm{app}}|$, computed from (22) ((*b*) and (*d*)) in the plane of the scaled variables ξ, τ (equation (21)), for $a = 4$, $N = 20$.

For ψ_{app}, the saddle-point method can be implemented explicitly. There are two saddles, $\xi_{\pm}(\xi, \tau)$, given by

$$\begin{aligned} &\partial_{\xi'}\Phi_{\mathrm{app}}(\xi', \xi, \tau) = 0 \Rightarrow \\ &\xi' = \xi_{\pm}(\xi, \tau) = \tfrac{1}{2}(\xi + \mathrm{i} \pm \mathrm{i}\sqrt{1 - \xi^2 + 2\mathrm{i}(\xi - 2\tau)}). \end{aligned} \tag{23}$$

For small τ, and with a natural convention for the square root, the saddle close to ξ, which we expect to be the main contribution, is the solution $\xi_{-}(\xi, \tau)$. For general ξ, τ, the saddle-point approximation is

$$\psi_{\mathrm{app,sp}}(\xi, \tau) = \sum_{\pm} a_{\pm} \frac{\exp\{\mathrm{i}N\Phi_{\mathrm{app}\pm}(\xi, \tau)\}}{\sqrt{1 + \tau\,\partial_{\xi} q_{\mathrm{app}}(\xi_{\pm}(\xi, \tau))}}, \tag{24}$$

where

$$\Phi_{\mathrm{app}\pm}(\xi, \tau) \equiv \Phi_{\mathrm{app}}(\xi_{\pm}(\xi, \tau), \xi, \tau). \tag{25}$$

The multiplier $a_{\pm}$ is 1 if the saddle $\pm$ contributes, and zero if it does not—a tricky matter that we explain now.

The deportment of the saddles divides the ξ, τ plane into regions, according to two criteria. At typical points, the contributions $\exp\{\mathrm{i}N\Phi_{\mathrm{app},\pm}\}$ differ exponentially in absolute value; there are regions where + dominates −, and vice versa. These are separated by 'anti-Stokes lines', where the absolute values of the exponentials are equal. Also important are 'Stokes lines', where the absolute values are maximally different; the importance of these lines of extreme dominance is that across them the subdominant (small) exponential can appear or disappear whilst 'hidden' behind the dominant one [16–18]—a phenomenon central to exponential

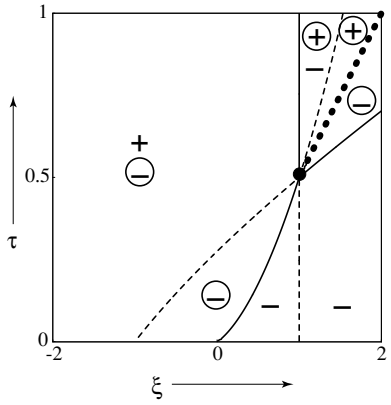

Figure 6. Structure of the ξ, τ plane according to the saddle-point approximation. Full curves: anti-Stokes lines; dashed curves: Stokes lines; dotted line: branch cut; black dot: saddle coalescence; + and −: contributing saddles, with the dominant saddle encircled. The Stokes and anti-Stokes lines were computed numerically using (26).

asymptotics [19]. In addition, the square root in (23) introduces a branch cut, across which the + and − contributions interchange. These three types of line are determined by

$$\begin{aligned} \text{anti-Stokes line:}\quad & \mathrm{Im}[\Phi_{\mathrm{app}+}(\xi,\tau)-\Phi_{\mathrm{app}-}(\xi,\tau)]=0 \\ \text{Stokes line:}\quad & \mathrm{Re}[\Phi_{\mathrm{app}+}(\xi,\tau)-\Phi_{\mathrm{app}-}(\xi,\tau)]=0 \\ \text{branch cut:}\quad & \text{argument of } \sqrt{\ } \text{ in (20) negative real} \\ & \Rightarrow \tau>0.5, \quad \xi=2\tau. \end{aligned} \tag{26}$$

Figure 6 shows how the ξ, τ plane is structured by these lines. The dominant feature from which all the lines issue is the point $\xi = 1$, $\tau = 1/2$ where the two saddles coalesce. We will describe the associated structure by proceeding clockwise round a circuit from the bottom right of the picture, where only − contributes, although it is subdominant, because there is no accompanying + exponential.

In fact, − contributes all the way across the small τ part of the plane, but in ways that are not obvious, as will now be explained. Moving left from the bottom right we cross a Stokes line, and − persists because the + saddle, that would otherwise dominate, is absent. Further left, we cross an anti-Stokes line; now − is the larger exponential, but still there is no +. The + exponential finally appears further to the left, on crossing the second Stokes line, and contributes along with −, but its contribution is subdominant.

This situation (both + and − contributing, with – dominant) continues round the circuit as τ increases, until the next anti-Stokes line is encountered, at $\tau > 1/2$, $\xi = 1$. As we will soon see, this is the most important event in the circuit. Crossing this anti-Stokes line moving to the right, + becomes dominant; soon afterwards, a Stokes line is crossed and the now-subdominant − saddle disappears, leaving only the dominant +. The next event is crossing the branch cut, across which + changes into −, which is still dominant. Finally, an anti-Stokes line is crossed, and −, contributing by itself, becomes subdominant as we close the circuit and return to the initial region.

Figure 7 illustrates the accuracy of the saddle-point approximation when calculated as just described. Even the inevitable failure when $\tau = 1/2$, through the saddle coalescence at $\xi = 1$ where the approximation diverges because of the vanishing of the denominator in (24), is barely visible in figure 7(*b*) and the magnification in (*c*).

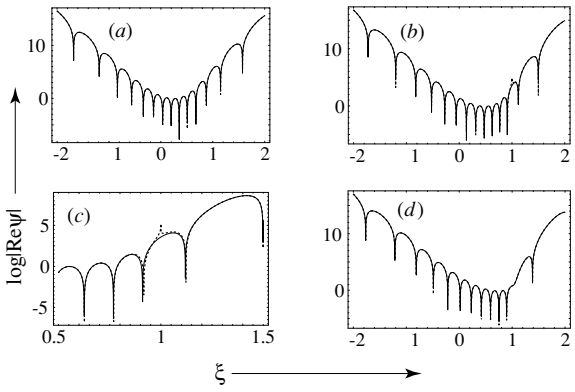

Figure 7. Full curves: $\log|\mathrm{Re}\,\psi_{\mathrm{app}}(\xi,\ \tau)|$ (equation (22)); dashed curves: saddle-point approximation $\log|\mathrm{Re}\,\psi_{\mathrm{app,sp}}(\xi,\tau)|$ (equation (24)), for (*a*) $\tau = 0.25$; (*b*) $\tau = 0.5$; (*c*) magnification of (*b*); (*d*) $\tau = 0.75$.

In understanding the 'wall' phenomenon and the disappearance of superoscillations, the exchange of dominance on crossing the anti-Stokes line $\xi = 1$, $\tau > 1/2$ is of central importance, because the associated wavenumber that appears is smaller than the superoscillatory wavenumber that it replaces. This explains the 'wall', clearly visible at $\xi = 1$ in figure 7(*d*). At the wall itself, the two wavenumbers are

$$k_{\mathrm{app}\pm}(1,\tau) \equiv \mathrm{Re}\,q_{\mathrm{app}}(\xi_{\pm}(1,\tau),1,\tau) = \frac{1 \mp \sqrt{2\tau - 1}}{2\tau}. \tag{27}$$

At $\tau = 1/2$, when the wall starts, $k_{\mathrm{app}+} = k_{\mathrm{app}-} = 1$, which happens to be the superoscillatory value in the scaled variables. Higher up the wall, both wavenumbers decrease, with the dominant value $k_{+\mathrm{app}}$ decreasing faster and becoming negative when $\tau > 1$, indicating a wave travelling to the left.

With equation (27) we are at last able to answer the question, posed at the beginning, of when the superoscillations disappear. This happens at the time τ_{d} when the larger wavenumber $k_{\mathrm{app}-}$ decreases to the value corresponding to the maximum Fourier component in the original $f(x)$. The scaling (21) shows that this corresponds to $k_{\mathrm{app}} = 1/a$. From (27),

$$k_{\mathrm{app}-}(1,\tau_{\mathrm{d}}) = \frac{1}{a} \quad \Rightarrow \quad \tau_{\mathrm{d}} = \frac{a^2}{4}\left(1 + \frac{2}{a}\sqrt{1 + \frac{4}{a} - \frac{4}{a^2}}\right) \underset{a\gg 1}{\rightarrow} \frac{a^2}{2}. \tag{28}$$

In the original variable t, this corresponds to the superoscillation disappearance time

$$t_{\mathrm{d}} = \frac{1}{4}\left(1 + \frac{2}{a} + \sqrt{1 + \frac{4}{a} - \frac{4}{a^2}}\right) \underset{a\gg 1}{\rightarrow} \frac{1}{2}. \tag{29}$$

Note that t_{d} depends only on a, and the dependence is weak; in particular, t_{d} is independent of N, and therefore, much smaller than the quantum revival time $N\pi/2$.

The foregoing arguments involve the particular superoscillatory initial state (1). However, we expect that our interpretation of the disappearance of superoscillations, in terms of complex momenta, will apply more generally. The reason is that for any initial quantum state the evolution can be described by an integral, analogous to the first equality in (15). Moreover, if the state is superoscillatory there will be a large parameter, analogous to N, so the integrand will vary quickly in modulus and phase, justifying the application of asymptotics, leading to the evolution being dominated by complex saddles, that is complex momenta. This deserves further study.

5. Diffraction grating analogue

One possible way to explore the evolution experimentally exploits the fact that $f(x)$ is periodic and so can represent a diffraction grating that transforms an incident plane of light or massive quantum particles (e.g. neutrons) into a propagating series of diffracted beams. In the case of light, such a grating could be manufactured by programming a spatial light modulator [20].

Let a plane wave with wavelength $\lambda = 2\pi/K$, propagating freely in the z direction, encounter a grating at $z = 0$, with spatial period πd, that transforms the wave to the superoscillatory function

$$\Psi(x, 0) = f(x/d). \tag{30}$$

We stipulate that there are no evanescent waves in the half-space $z > 0$; the condition for this is $K > N/d$. On the other hand, we want the superoscillations in the grating to be smaller than λ, so that $K < aN/d$. These conditions, namely

$$\frac{aN}{d} > K > \frac{N}{d}, \tag{31}$$

generate a grating with a sub-wavelength structure, producing a field that nevertheless consists entirely of propagating (nonevanescent) waves. Therefore this grating produces an unfamiliar kind of superresolution (sub-wavelength structure in the field), namely superresolution without evanescent waves. We will investigate how far into the field the superoscillations propagate.

The field beyond the grating is the exact solution of the Helmholtz equation with wavenumber K, starting with (30), namely (after removing a trivial phase factor)

$$\Psi(x, z) = \exp(-\mathrm{i}Kz) \sum_{m=0}^{N} c_m \exp\left\{\mathrm{i}\left(Nk_m x/d + z\sqrt{K^2 - N^2k_m^2/d^2}\right)\right\}. \tag{32}$$

If the second inequality in (31) is strong, that is if the highest Fourier components of the grating vary much more slowly than λ, all propagation angles $\theta_m = \arcsin(Nk_m/dK)$ are small, and it is tempting to replace by its paraxial approximation, namely

$$\begin{aligned}\Psi_{\text{paraxial}}(x, z) &= \sum_{m=0}^{N} c_m \exp\left\{\mathrm{i}N\left(k_m x/d - zNk_m^2/2Kd^2\right)\right\} \\ &= \psi\left(\frac{x}{d}, z\frac{N}{Kd^2}\right),\end{aligned} \tag{33}$$

where ψ is given by (15).

By this procedure, the question of propagation of superoscillations beyond the grating is reduced to the question already studied, of the persistence of superoscillations under quantum evolution. The periodicity of ψ, representing quantum revivals, is now reinterpreted as the Talbot effect [21–23] in diffraction theory: reproduction of the form of a grating at multiples of the Talbot distance

$$z_{\text{Talbot}} = \frac{1}{2}\pi K d^2 = \frac{(\text{grating period})^2}{\lambda}. \tag{34}$$

But since superoscillations are so delicate, it is imperative to know whether they are destroyed by non-paraxial effects. Figures 8 and 9 indicate that this does not happen, as we discuss in more detail later. The situation depicted, where $d = 1$, $a = 8$, $N = 10$, $K = 40$, corresponds to a grating with maximum propagation angle $\theta_{\max} \sim \arcsin(1/4) \sim 15^\circ$, which is paraxial but not extremely so, with the shortest spatial scale $d\pi/N = 2\lambda$ in its Fourier series, and with a superoscillatory fine structure with spatial scale $d\pi/Na = \lambda/4$.

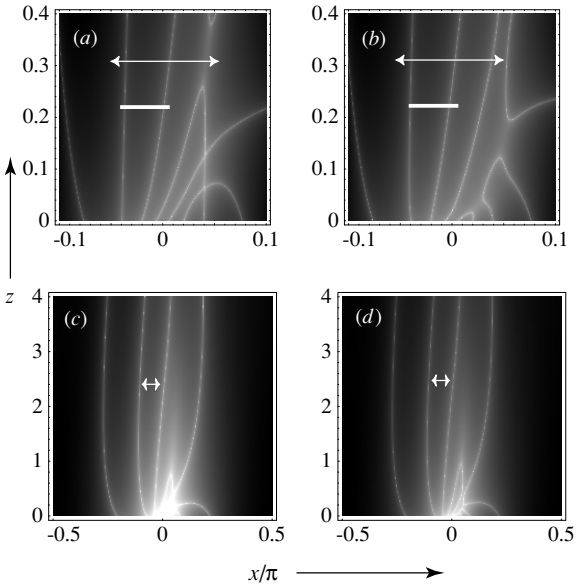

Figure 8. Density plots of waves beyond a superoscillatory diffraction grating, for $d = 1$, $a = 8$, $N = 10$, $K = 40$ ((*a*) and (*c*)) paraxial wave $-\log|\mathrm{Re}\ \Psi_{\mathrm{parax}}|$ (equation (33)); ((*b*) and (*d*)) as (*a*), for the exact diffracted wave $-\log|\mathrm{Re}\ \Psi|$ (equation (32)). As before, double-headed arrows mark the shortest period $d\pi/N = \pi/10$ in the Fourier series; in (*a*) and (*b*), the bars mark the wavelength $\lambda = 2\pi/K = \pi/20$.

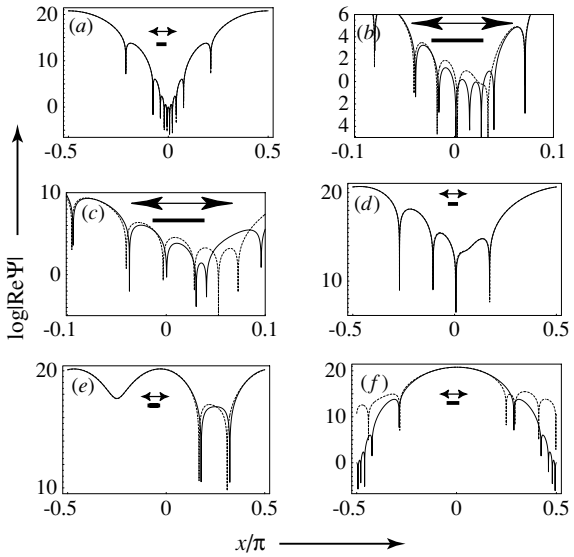

Figure 9. Full curves: paraxial wave $\log|\mathrm{Re}\ \Psi_{\mathrm{parax}}|$; dashed curves: exact waves $\log|\mathrm{Re}\ \Psi|$, for $d = 1$, $a = 4$, $N = 10$, $K = 40$, and (*a*) $z = 0$; (*b*) $z = 1/32$ (coalescence of saddles (section 4)); (*c*) $z = z_\lambda = 0.213$ (superoscillations expand to λ); (*d*) $z = z_{\mathrm{d}} = 2.449$ (disappearance of superoscillations); (*e*) $z = z_{\mathrm{T}}/2 = 10\pi$ (half the Talbot repetition distance); (*f*) $z = z_{\mathrm{T}} = 20\pi$ (Talbot repetition distance). Double-headed arrows and bars as in figure 8.

For the grating wave, the physically important propagation range is the distance z_λ, below which the superoscillatory fine structure remains smaller than the wavelength. This can be

derived from (27), as the condition for the scaled wavenumber $k_{\rm app}$ at the left of the 'wall' to fall to the value Kd/Na; a short calculation gives

$$z_\lambda = \frac{N}{4K}\left(1+\frac{2Kd}{Na}+\sqrt{1+\frac{4Kd}{Na}-4\left(\frac{Kd}{Na}\right)^2}\right)\underset{a\gg 1}{\rightarrow}\frac{N}{2K}=\frac{N\lambda}{4\pi}. \tag{35}$$

This distance depends only weakly on the degree of superoscillation a, but depends strongly on the asymptotic parameter N.

We should compare z_λ with the persistence distance of ordinary evanescent waves with transverse wavenumber aN/d, corresponding to the fastest superoscillation. Such waves have the form $\exp(\mathrm{i}aNx/d)\exp(-z\sqrt{(aN/d)^2-K^2})$, so the persistence distance, beyond which the waves have decayed below $1/e$ of their original intensity, is

$$z_{\rm evanescence}=\frac{1}{2\sqrt{(aN/d)^2-K^2}}\underset{a\gg 1}{\rightarrow}\frac{d}{2Na}<\frac{1}{2K}. \tag{36}$$

Thus,

$$z_\lambda/z_{\rm evanescence} > N \gg 1, \tag{37}$$

and we conclude that, for propagating sub-wavelength structure, gratings based on superoscillations are much more effective than the more familiar ones based on evanescent waves.

Analogous to the quantum superoscillation disappearance time $t_{\rm d}$ (equation (29)) is the distance $z_{\rm d}$, where the superoscillations have expanded to the spatial scale of the largest Fourier component in the grating. This is

$$z_{\rm d}=\frac{Kd^2}{4N}\left(1+\frac{2}{a}+\sqrt{1+\frac{4}{a}-\frac{4}{a^2}}\right)\underset{a\gg 1}{\rightarrow}\frac{Kd^2}{2N}. \tag{38}$$

The proliferation of significant propagation distances associated with these gratings might be confusing, so here is a summary, together with the numerical values (in brackets) for the parameters of figures 8 and 9:

$$\begin{array}{ll}
z=0; & \text{inital superoscillation}\\
z=\dfrac{d^2K}{2Na^2}\left(=\dfrac{1}{32}\right); & \text{coalescence of saddles (complex momenta)}\\
z=z_\lambda(=0.213); & \text{oscillations reach wavelength scale (equation (35))}\\
z=z_{\rm d}(=2.449); & \text{superoscillations disappear (equation (38))}\\
z=z_{\rm Talbot}(=20\pi); & \text{Talbot repetition distance (equation (34)).}
\end{array} \tag{39}$$

Finally, we discuss the comparison of the paraxial and exact fields in figures 8 and 9. Figures 8(*a*) and (*b*) show slight differences between the fields over the range in which superoscillations expand to the external wavelength scale, but the differences do not destroy our conclusion about the effectiveness of superoscillatory gratings for propagating sub-wavelength structure. Over the larger distance depicted in figures 8(*c*) and (*d*)), including the range in which superoscillations disappear, differences are barely perceptible.

The more discriminating comparisons in figure 9 show that the main differences between the paraxial and exact waves occur in the exponentially weak regions of the field. For the smaller distances corresponding to saddle coalescence (figure 9(*b*)) and z_λ (figure 9(*c*)), there is some nonparaxial corruption of the superoscillations, but they are not destroyed. For $z_{\rm d}$ (figure 9(*d*)), the differences are barely distinguishable, and this agreement extends to great

distances, including $z_{\text{Talbot}}/2$ (figure 9(*e*)). At z_{Talbot} itself (figure 9(*f*)), the exact diffracted wave does not reproduce the superoscillations, but the parts of the pattern that are not exponentially small are correctly reproduced.

Acknowledgment

MVB's research is supported by The Royal Society.

References

[1] Aharonov Y, Popescu S and Rohrlich D 1990 How can an infra-red photon behave as a gamma ray? Tel-Aviv University *Preprint* TAUP 1847–90 (paper in preparation, 2006)
[2] Aharonov Y and Vaidman L 1990 Properties of a quantum system during the time interval between measurements *Phys. Rev.* A **41** 11–20
[3] Aharonov Y, Anandan J, Popescu S and Vaidman L 1990 Superpositions of time evolutions of a quantum system and a quantum time-translation machine *Phys. Rev. Lett.* **64** 2965–8
[4] Aharonov Y, Popescu S, Rohrlich D and Vaidman L 1993 Measurements, errors and negative kinetic energy *Phys. Rev.* A **48** 4084–90
[5] Berry M V 1994 Evanescent and real waves in quantum billiards, and Gaussian Beams *J. Phys. A: Math. Gen.* **27** L391–L398
[6] Berry M V 1994 Faster than Fourier in Quantum Coherence and Reality *Celebration of The 60th Birthday of Yakir Aharonov* ed J S Anandan and J L Safko (Singapore: World Scientific) pp 55–65
[7] Popescu S 1991 Multi-time and non-local measurements in quantum mechanics *PhD Thesis* Physics Department, Tel-Aviv University
[8] Bucklew J A and Saleh B E A 1985 Theorem for high-resolution high-contrast image synthesis *J. Opt. Soc. Am.* A **2** 1233–6
[9] Kempf A and Ferreira P J S G 2004 Unusual properties of superoscillating particles *J. Phys. A: Math. Gen.* **37** 12067–76
[10] Calder M S and Kempf A 2005 Analysis of superoscillatory wave functions *J. Math. Phys.* **46** 012101-1–18
[11] Eberly J H, Narozhny N B and Sanchez-Mondragon J J 1980 Periodic spontaneous collapse and revival in a simple quantum model *Phys. Rev. Lett.* **44** 1323–6
[12] Leichtle C, Averbukh I S and Schleich W P 1996 Generic structure of multi-level quantum beats *Phys. Rev. Lett.* **77** 3999–4002
[13] Yeazell J A and Stroud C R J 1991 Observation of fractional revivals in the evolution of a Rydberg atomic wave packet *Phys. Rev.* A **43** 5153–6
[14] de Bruijn N G 1958 *Asymptotic Methods in Analysis* (Amsterdam: North-Holland)
de Bruijn N G 1981 *Asymptotic Methods in Analysis* (New York: Dover) (reprinted)
[15] Wong R 1989 *Asymptotic Approximations to Integrals* (New York: Academic)
[16] Berry M V 1989 Uniform asymptotic smoothing of Stokes's discontinuities *Proc. R. Soc.* A **422** 7–21
[17] Berry M V 1989 Stokes' phenomenon; smoothing a Victorian discontinuity *Publ. Math. Institut Hautes Études Scientifique* **68** 211–21
[18] Stokes G G 1864 On the discontinuity of arbitrary constants which appear in divergent developments *Trans. Camb. Phil. Soc.* **10** 106–28
[19] Berry M V 1992 *Asymptotics, Superasymptotics, Hyperasymptotics in Asymptotics Beyond All Orders* ed H Segur and S Tanveer (New York: Plenum) pp 1–14
[20] Hamamatsu 2005 http://sales.hamamatsu.com/en/products/electron-tube-division/detectors/spatial-light-modulator/applications.php?& view = applications
[21] Berry M V and Klein S 1996 Integer, fractional and fractal Talbot effects *J. Mod. Opt.* **43** 2139–64
[22] Berry M V, Marzoli I and Schleich W P 2001 Quantum carpets, carpets of light *Phys. World* **14** 39–44
[23] Talbot H F 1836 Facts relating to optical science: No IV *Phil. Mag.* **9** 401–7